Control of heart rate by cAMP sensitivity of HCN channels

Jacqueline Alig[a], Laurine Marger[b], Pietro Mesirca[b], Heimo Ehmke[c], Matteo E. Mangoni[b], and Dirk Isbrandt[a,1]

[a]Experimental Neuropediatrics, Center for Obstetrics and Pediatrics & Center for Molecular Neurobiology, University Medical Center Hamburg-Eppendorf, 20246 Hamburg, Germany; [b]CNRS UMR 5203, Inserm U661; University Montpellier I & II, Institute of Functional Genomics, Department of Physiology, 34094 Montpellier Cedex 05, France; and [c]Department of Vegetative Physiology and Pathophysiology, Center for Experimental Medicine, University Medical Center Hamburg-Eppendorf, 20246 Hamburg, Germany

Edited by William A. Catterall, University of Washington School of Medicine, Seattle, WA, and approved May 22, 2009 (received for review October 16, 2008)

"Pacemaker" f-channels mediating the hyperpolarization-activated nonselective cation current I_f are directly regulated by cAMP. Accordingly, the activity of f-channels increases when cellular cAMP levels are elevated (e.g., during sympathetic stimulation) and decreases when they are reduced (e.g., during vagal stimulation). Although these biophysical properties seem to make f-channels ideal molecular targets for heart rate regulation by the autonomic nervous system, the exact contribution of the major I_f-mediating cardiac isoforms HCN2 and HCN4 to sinoatrial node (SAN) function remains highly controversial. To directly investigate the role of cAMP-dependent regulation of hyperpolarization activated cyclic nucleotide activated (HCN) channels in SAN activity, we generated mice with heart-specific and inducible expression of a human *HCN4* mutation (573X) that abolishes the cAMP-dependent regulation of HCN channels. We found that hHCN4–573X expression causes elimination of the cAMP sensitivity of I_f and decreases the maximum firing rates of SAN pacemaker cells. In conscious mice, hHCN4–573X expression leads to a marked reduction in heart rate at rest and during exercise. Despite the complete loss of cAMP sensitivity of I_f, the relative extent of SAN cell frequency and heart rate regulation are preserved. Our data demonstrate that cAMP-mediated regulation of I_f determines basal and maximal heart rates but does not play an indispensable role in heart rate adaptation during physical activity. Our data also reveal the pathophysiologic mechanism of hHCN4–573X–linked SAN dysfunction in humans.

bradycardia | hyperpolarization cyclic nucleotide–gated ion channels | pacemaker activity | sinoatrial node | transgenic mice

Heart automaticity is a fundamental physiological function in higher organisms. The dominant pacemaker of mammalian hearts is the sinoatrial node (SAN). Dysfunction or failure of SAN activity in humans may lead to an abnormally low heart rate, causing such symptoms as palpitations, fatigue, and syncope, which eventually require implantation of a pacemaker device (1). Elevated resting heart rate, in contrast, is associated with increased cardiovascular mortality and morbidity (2, 3). Despite the importance of cardiac pacemaking as a physiological process, the complex mechanisms underlying SAN automaticity and heart rate regulation remain incompletely understood. SAN activity is controlled by the autonomic nervous system; cholinergic and β-adrenergic stimulation either slows or accelerates spontaneous SAN activity. Several ionic currents contribute to cardiac automaticity (4–6). Some of these currents are targets of regulation by the autonomic nervous system, but their physiological importance is a matter of debate (4, 5). "Pacemaker" f-channels mediating the hyperpolarization-activated nonselective cation current I_f, in particular, are directly regulated by cAMP (7). These channels are homotetrameric or heterotetrameric complexes of hyperpolarization-activated cyclic nucleotide-gated (HCN) subunits (8). cAMP binds to the cyclic nucleotide-binding domain (CNBD) and elicits a positive shift in the voltage dependence of activation. Accordingly, the activity of f-channels increases when cellular cAMP levels are elevated (e.g., during sympathetic stimulation) and decreases when they are reduced (e.g., during vagal stimulation) (8). Although these biophysical properties seem to make f-channels ideal molecular targets for heart rate regulation, the contribution of the major I_f-mediating cardiac isoforms HCN2 and HCN4 to SAN function remains highly controversial. Although human genetic (9–12) and pharmacologic (5, 13, 14) studies suggest a significant role for HCN4 subunits in SAN pacemaking in humans and rodents, recent data from transgenic mouse models have challenged this view (15, 16). Targeted deletion of *HCN4* in adult mice was found to cause heart rate–dependent sinus pauses but to have no effect on either basal or maximal heart rate or heart rate regulation (16). Surprisingly similar observations were made in adult heterozygous knock-in mice expressing a cAMP binding–deficient HCN4 subunit (15). Furthermore, targeted deletion of *HCN2* caused sinus dysrhythmia, but did not alter heart rates (17).

Our study was designed to investigate the role of cAMP-dependent modulation of HCN channels in heart rate regulation. Furthermore, we aimed to elucidate the pathophysiologic mechanisms underlying dysfunction or failure of SAN activity associated with a *HCN4* mutation (573X) that abolishes cAMP sensitivity of HCN4 channels (12). Toward this end, we generated transgenic mice with heart-specific and inducible expression of hHCN4–573X and determined the role of cAMP-mediated regulation of HCN channel activity in SAN function.

Results

Generation of Conditional hHCN4–573X Transgenic Mice. We generated transgenic mice with alpha-myosin heavy-chain (αMHC) promoter and Tet-Off system–controlled cardiac-specific expression (18, 19) of an engineered HCN4 subunit carrying a human mutation that we had previously identified in a patient with SAN dysfunction (hHCN4–573X; Fig. 1*A*) (12). The mutation results in deletion of the CNBD from HCN4 subunits and causes cAMP insensitivity of heterologously coexpressed wild-type HCN4 subunits in a dominant-negative manner (12). The extent of αMHC promoter–driven transgene expression in the murine SAN region was assessed by crossbreeding αMHC-tTA promoter mice (18) with mice expressing EGFP under control of a bidirectional tetracycline-response element (20). Examination of EGFP autofluorescence in excised atria from double-transgenic animals revealed strong signals in central and peripheral SAN areas (Fig. 1*B*) and acutely isolated SAN pacemaker cells (data not shown), indicating that αMHC-tTA promoter mice are well suited to direct transgene expression to the SAN.

Author contributions: J.A., H.E., M.M., and D.I. designed research; J.A., L.M., P.M., M.M., and D.I. performed research; J.A., L.M., P.M., M.M., and D.I. analyzed data; and J.A., H.E., M.M., and D.I. wrote the paper.

The authors declare no conflict of interest.

This article is a PNAS Direct Submission.

[1]To whom correspondence should be addressed. E-mail: dirk.isbrandt@isbrandtlab.org.

This article contains supporting information online at www.pnas.org/cgi/content/full/0810332106/DCSupplemental.

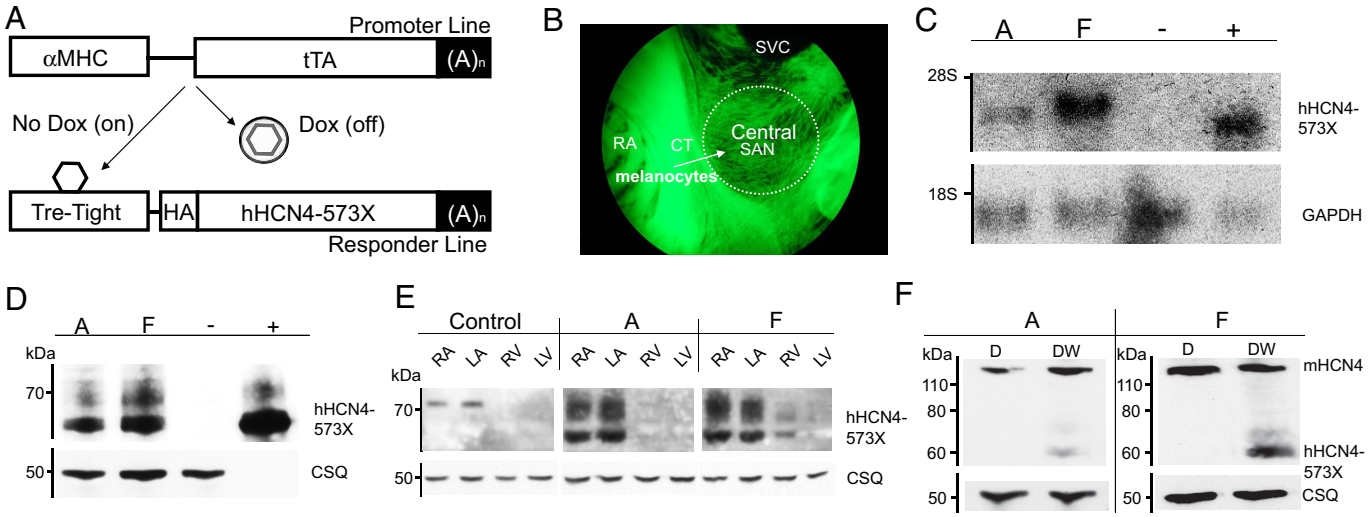

Fig. 1. Generation and characterization of transgenic mice. (*A*) Schematic illustration of the Tet-Off system. (*B*) Fluorescence microscopic images (EGFP autofluorescence) of the SAN region of an αMHC-tTA–driven EGFP indicator line (20). (*C*) Northern blot detection of hHCN4–573X–specific RNA in total cardiac RNA samples from offspring of 2 independent founder lines (A and F) revealing 2 different expression levels. Total RNA isolated from a wild-type mouse heart was used as a negative control (''−''). In vitro–synthesized hHCN4 cRNA (100 pg) was added to the control RNA as a positive control (''+''). (*D*) Western blot detection of transgenic hHCN4–573X proteins in total heart tissue lysates from double-transgenic (mutant) offspring of both founder lines and from a nontransgenic control mouse (''−''). Total lysates of human embryonic kidney (HEK-293) cells transiently transfected with hHCN4–573X were used as a positive control (12). (*E*) Region-specific Western blot analysis of proteins isolated from the right atrium (RA), left atrium (LA), right ventricle (RV), and left ventricle (LV). hHCN4–573X protein was detectable in atrial tissue lysates from both founder lines, whereas ventricular transgene expression was detected only in line F. (*F*) DOX-dependent regulation of hHCN4–573X expression and comparison with endogenous mHCN4 protein levels analyzed by Western blot. Total heart lysates were obtained from mutants on DOX (''D'') and from DOX-water (''DW'') animals. Abbreviations: tTA, Tet-Off system transactivator; Tre, tetracycline-responsive element; CT, crista terminalis, SVC, superior vena cava.

We analyzed the levels of αMHC promoter–driven expression of hHCN4–573X mRNA and protein in the hearts of double-transgenic mice from 2 independent founder lines (A and F). Animals of both lines expressed detectable levels of transgene-specific mRNA (Fig. 1*C*) or protein (Fig. 1*D*) in heart tissue, although to different extents. The expression of hHCN4–573X was higher in line F mice than in line A mice. In both founder lines, hHCN4–573X immunoreactivity was high in the atria and almost absent in ventricles (Fig. 1*E*). In both lines, the use of the Tet-Off system was functional, as indicated by efficient suppression of transgene expression by the addition of doxycycline (DOX) to the drinking water (Fig. 1*F*). After DOX withdrawal, transgene expression was restored after 4 weeks in the line F mice and after 6 weeks in the line A mice. Compared with endogenous mHCN4 protein levels, hHCN4–573X expression was lower in the line A mice and almost identical in the line F mice (Fig. 1*F*).

Double-transgenic mutants (without DOX treatment) from both founder lines were born at Mendelian ratios and were viable. Echocardiography showed normal ventricular size and function in

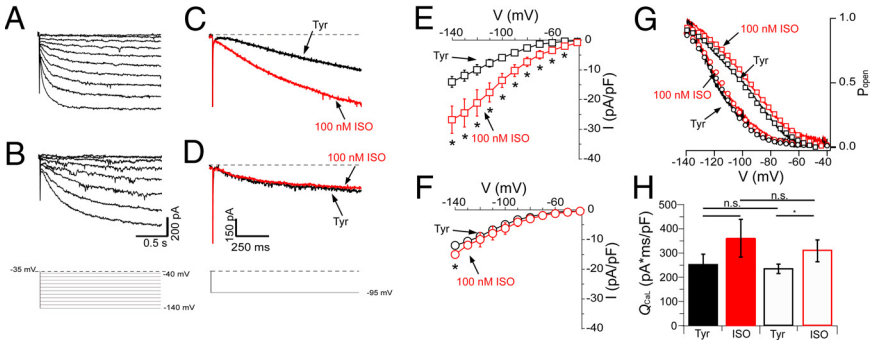

Fig. 2. β-adrenergic regulation of I_f in control and mutant SAN cells. Black indicates recording under control conditions with normal Tyrode's solution (Tyr); red indicates data obtained after ISO stimulation. (*A* and *B*) Examples of representative voltage-clamp recordings of hyperpolarization-induced currents from acutely isolated control (*A*) or mutant (*B*; founder line A) SAN pacemaker cells (protocol shown below traces). (*C* and *D*) Sample traces of control (*C*) and mutant I_f (*D*) in the absence or presence of 100 nM ISO. (*E* and *F*) Current density–voltage relationships at baseline revealing comparable I_f densities in control (black squares) and mutant cells (black circles). Stimulation with 100 nM ISO increased I_f density in control cells (*E*, red squares), but not in mutant cells (*F*, red circles). (*G*) I_f activation curves in control (black squares) and mutant cells (black circles) (26). I_f in mutant cells activated at more negative voltages than in control cells. In control cells, application of ISO caused a significant shift in the I_f activation curve to more positive voltages (red squares). In contrast, no significant ISO-dependent shift was observed in mutant cells (red circles). (*H*) Analysis of β-adrenergic regulation of $I_{Ca,L}$ in control and mutant cells. The bar graph shows current–time integrals of $I_{Ca,L}$. $I_{Ca,L}$ obtained from the same set of experiments shown in (*C*–*F*). $I_{Ca,L}$ was activated by depolarizing voltage steps from a holding potential of −60 mV to −35 mV. At this test voltage, $I_{Ca,L}$ is generated predominantly by $Ca_V1.3$ channels (29). $I_{Ca,L}$ was recorded in normal Tyrode's solution (Tyr) at 35 °C with and without 100 nM ISO. $I_{Ca,L}$ in control ($n = 5$; filled bars) and mutant SAN cells ($n = 5$; open bars) was similarly stimulated by application of ISO. $I_{Ca,L}$ waveform was integrated over a time interval of 60 ms starting from the current onset (30). $^*P < .05$.

Table 1. Properties of I_f in SAN cells of control and mutant mice

		Controls		Mutants		*P*	*P*
	Parameter	(A)	*n*	(B)	*n*	A versus B	C versus D
	Cell capacitance, pF	24 ± 2	17	30 ± 2	28	.0692	
	I_f current density, pA/pF	−14.0 ± 1.8	6	−12.00 ± 0.14	14	.6579	
(C)	*$V_{1/2}$ activation, baseline, mV*	−101 ± 3	6	−121 ± 3	10	.0053	.0312 (A) .6221 (B)
	Slope factor, baseline	15.8 ± 1.7	6	13.0 ± 1.9	10	.3463	.4095 (A) .0752 (B)
	τ_{act} baseline, ms	428 ± 65	7	1195 ± 169	7	.0019	.0234 (A) .1040 (B)
(D)	*$V_{1/2}$ activation, ISO, mV*	−92 ± 2	7	−123 ± 4	6	<.0001	
	Slope factor, ISO	17.7 ± 1.4	7	19.3 ± 3.0	6	.6165	
	τ_{act} ISO, ms	371 ± 66	7	1780 ± 413	7	.0103	

Values are given ± SEM. Differences in parameters between groups were tested using an unpaired Student *t* test. Current density values were measured at a test potential of −140 mV. Activation time constants were measured at the corresponding I_f half-activation voltage ($V_{1/2}$) in each mouse strain (−100 in control cells and −120 mV in mutant cells). Note that ISO (100 nM) did not elicit a positive shift in the $V_{1/2}$ or accelerate the I_f activation kinetics in mutant SAN cells (line A).

the line F mutants [supporting information (SI) Fig. S1*A–E*], which had detectable levels of hHCN4–573X in their ventricles (Fig. 1*E*). The left ventricular mass to body weight and atrial mass to body weight ratios were normal as well (Fig. S1 *F* and *G*).

hHCN4–573X Expression Eliminates cAMP Sensitivity of I_f and Affects SAN Pacemaker Cell Activity. To characterize the consequences of hHCN4–573X expression on the properties of SAN pacemaker cells, we obtained perforated patch-clamp recordings from acutely isolated SAN cells (line A, without DOX treatment). Compared with controls, I_f recorded from mutant cells exhibited similar current densities but slower activation kinetics (Fig. 2*A* and *B*). In addition, I_f was insensitive to β-adrenergic stimulation with isoproterenol (ISO) across the entire voltage range tested (Fig. 2*C–G*; Table 1). The I_f half-activation voltage ($V_{½}$) recorded from mutant SAN cells was about 20 mV more negative than that of control SAN cells and did not respond to ISO stimulation (Fig. 2*G*; Table 1), resulting in an I_f activation range beyond physiologically relevant diastolic membrane potentials, that is, negative to that spanning the diastolic depolarization (5). In contrast, the ISO response of the L-type Ca^{2+} current ($I_{Ca,L}$) was unaffected in mutant and control SAN cells (Fig. 2*H*).

The loss of ISO regulation of I_f was associated with profound changes in SAN cell automaticity. All SAN cells from control mice displayed regular and sustained pacemaker activity under basal conditions (no ISO stimulation, $n = 15$; Fig. 3*A* and *B*) and accelerated pacing rates after application of 2 nM and 100 nM ISO ($n = 12$; Fig. 3*A–C*). In contrast, only 2 of 18 mutant SAN cells tested displayed regular pacemaker activity under basal conditions; 11 cells were arrhythmic and alternated between action potentials and subthreshold membrane potential oscillations, and 5 cells were quiescent (Fig. 3*A*, *B*, and *D*). Application of ISO onto mutant SAN cells ($n = 10$) induced a dose-dependent acceleration of pacemaking similar to that observed in control cells (Fig. 3*C*). ISO application also resulted in restoration of regular pacemaker activity in arrhythmic mutant cells (Fig. 3*B*) and resumption of pacemaker activity in 3 of the 5 quiescent cells, thereby reducing the percentage of quiescent cells in the overall cell population (Fig. 3*D*). But even at a saturating concentration of ISO, the pacing rate of mutant SAN cells was significantly slower than that of controls (Fig. 3*C*; Table S1). Analysis of action potential properties in mutant SAN cells revealed a compound effect of hHCN-573X expression that included a strong reduction in the slope of diastolic depolarization, a more positive maximum diastolic potential, and prolonged action potential duration (Table 2). Analysis of ISO-induced diastolic currents in SAN cells from control and mutant mice in the presence of the selective I_f inhibitor ivabradine (IVA) revealed no significant differences (Fig. S2); however, under basal conditions, a small shift in total membrane current in the inward direction during the action potential (membrane potential between 0 and −20 mV) was seen (Fig. S2).

Taken together, our data indicate that an hHCN4–573X–linked

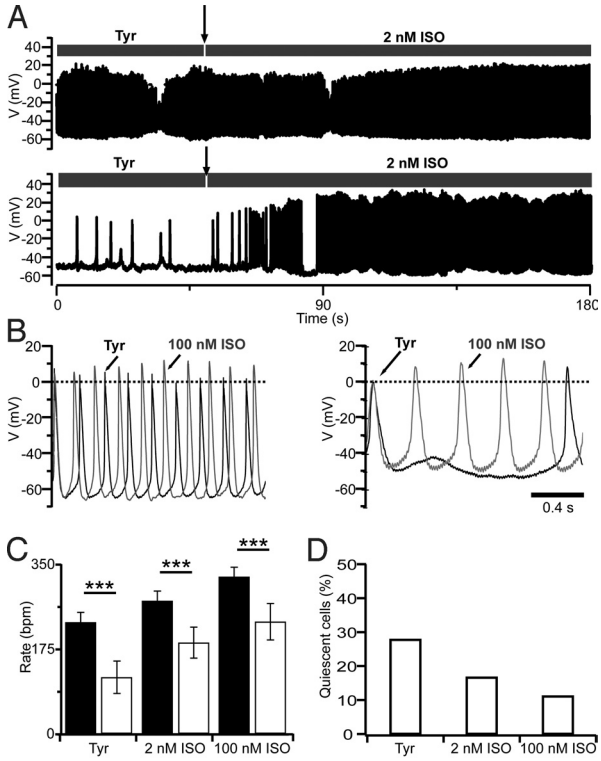

Fig. 3. Pacemaker activity in SAN cells of control and mutant mice. (*A*) Fast and regular firing was observed in SAN cells of control mice (*Top*), whereas most mutant (founder line A) SAN cells showed only intermittent action potential firing, alternating with oscillations in membrane voltage (*Bottom*). Activation of the β-adrenergic receptor by a submaximal dose of ISO (2 nM) restored regular firing in mutant cells, although at a slower rate than in control cells. (*B*) Fast-time scale recording of pacemaker activity of a control cell (*Left*) and a mutant cell (*Right*). Control cells showed a regular firing rate in Tyrode's solution (Tyr; black line) and accelerated firing in ISO (gray line). In most mutant cells, ISO application restored regular firing activity, but the maximum rate was still slower than that in control cells. (*C*) Pacemaker activity in mutant cells ($n = 10$; open bars) was increased by stimulation with 2 nM or 100 nM ISO, but the cell firing rate at each dose tested did not reach that of control cells ($n = 12$; filled bars). Note that the firing rate of mutant cells was reduced at baseline (Tyr) and at each ISO concentration tested (Table S1). (*D*) The percentage of quiescent pacemaker cells decreased in a dose-dependent manner on superfusion with 2 nM or 100 nM ISO. ***$P < .001$.)

PHYSIOLOGY

Table 2. Pacemaker activity and action potential properties in SAN cells of control and mutant mice

	Controls		Mutants		
Action potential parameter	SAN cells	*n*	SAN cells	*n*	*P*
Rate, bpm	247 ± 16	15	165 ± 32	10	.0209
Action potential amplitude, mV	81 ± 4	15	83 ± 3	10	.8228
Minimum diastolic potential, mV	−58 ± 1	15	−51 ± 2	10	.0036
Action potential duration, ms	112 ± 5	15	150 ± 15	10	.0139
Action potential threshold, mV	−45 ± 2	15	−35 ± 9	10	.1821
Slope of the diastolic depolarization, V/S	0.084 ± 0.014	15	0.019 ± 0.007	10	.0014

This table shows basal cellular pacemaker activity in the absence of ISO stimulation. Thus SAN cell firing rates differ from those shown in Fig. 3*C*. Cells from mutant animals that were completely quiescent ($n = 5$) and cells in which the slope of diastolic depolarization was too low to allow accurate measurement ($n = 3$) were excluded from this analysis. Differences in parameters between groups were tested using an unpaired Student *t* test. Values are given as mean ± SEM.

loss of cAMP sensitivity of f-channels causes impaired basal cellular automaticity and a reduction in the maximum firing rate of SAN pacemaker cells, but no elimination of β-adrenergic regulation of cellular automaticity.

Reduced Basal and Exercise-Induced Heart Rates in hHCN4–573X–Expressing Mice. To investigate how the cellular changes in isolated SAN pacemaker cells influence the heart rates of intact animals, we used ECG telemetry in conscious mice. First, we tested whether pharmacologic blockade of I_f differently affected the heart rate of mutants (line A, no DOX treatment) and controls using IVA (21). IVA inhibits f-channels by entering the intracellular side of the channel pore in a manner independent of cAMP binding to the CNBD (8). In the presence of IVA, blocking of I_f was comparable in the control and mutant SAN cells (Fig. 4*A*). The use of experimental doses of IVA in in vivo pilot experiments showed that IVA-induced heart rate reduction in the control mice was maximal at doses ranging from 3 to 6 mg/kg of body weight (data not shown). Intraperitoneal administration of 3 or 6 mg/kg IVA caused a significant decrease in heart rate in the controls (Fig, 4*B*). In striking contrast, IVA had no effect on heart rate in the mutants (Fig. 4*C*), demonstrating that the contribution of I_f to SAN function was specifically and completely eliminated by the hHCN4–573X transgene.

To avoid possible confounding effects of hHCN4–573X expression during development, additional mice were raised on DOX, implanted with the telemetry device, and then switched to water (DW mutants), to induce transgene expression (Fig. 5*A*). The activity-dependent heart rate was identical in the DW mutants and control mice (Fig. 5*B*). On DOX withdrawal, DW mutants, unlike controls, exhibited significantly lower heart rates at all activity levels (Fig. 5*C*). Surprisingly, the relative activity-induced increase in heart rate (i.e., the difference between maximum and minimum heart rates) was unchanged in these mice (Fig. 5*B–E*). These findings reveal the contribution of effectors of autonomic nervous system modulation of heart rate other than I_f, such as I_{KACh}, $I_{Ca,L}$, I_{st}, and ryanodine receptor–mediated Ca^{2+} release (5, 6). In line with this conclusion, the differences between mutants and controls were abolished by the pharmacologic blockade of autonomic nervous system–mediated heart rate regulation using atropine and propranolol (Fig. 5*D*). In addition, 24-hour heart rate histograms showed that the relative extent of SAN regulation was comparable in the control mice and DW mutants, although a marked left shift in the SAN frequency range was seen in DW mutants (Fig. 5*F* and *G*). This difference disappeared after the application of atropine and propranolol (Fig. 5*F* and *G*). No conduction abnormalities or SAN dysrhythmias were observed in the DW mutants on suppression of transgene expression by DOX administration, after DOX withdrawal (Figs. 5*H* and S3), or during pharmacologic autonomic nervous system–mediated blockade (data not shown).

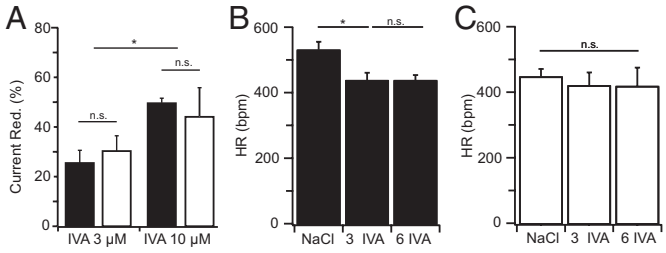

Fig. 4. The selective I_f inhibitor IVA reduced the heart rate in control mice, but not in mutant mice. (*A*) Application of 3 or 10 μM IVA onto acutely isolated control (filled bars) or mutant (open bars) SAN cells revealed similar I_f inhibition at a membrane potential of −105 mV. (*B* and *C*) Mean heart rate in control mice (*B*; $n = 3$) and mutant mice (*C*; $n = 4$). Each animal received an i.p. injection of physiological saline (0.9% NaCl), followed by IVA at a dose of 3 mg/kg (3 IVA) or 6 mg/kg (6 IVA) at 72-h intervals, to allow washout of the drug. The heart rate was measured for 3 h before injection of either NaCl or IVA and then for 3 h after injection. Note the reduced basal heart rate in the mutant mice. The aforementioned periods for heart rate averaging were selected because IVA reached its maximum effect 2 h after injection of 3 mg/kg and 1 h after injection of 6 mg/kg (data not shown). Data were compared using ANOVA and the Newman–Keuls posthoc test. $*P < .05$.

Discussion

SAN automaticity is generated through a complex interplay of membrane ion channels, spontaneous intracellular Ca^{2+} release, and transporters (4, 5). The relative contribution of these effectors to autonomic nervous system–mediated regulation of heart rate is a matter of debate (4, 5, 22). In particular, the role of HCN channels as the dominant mechanism in heart rate regulation has repeatedly been called into question (4, 23). Human genetic studies have suggested that HCN4 channels are important components of the SAN pacemaker machinery (9–12). A contribution of I_f to heart rate determination is further supported by the observation of a heart rate–lowering effect in both humans and rodents when I_f is specifically blocked with IVA (13, 14, 24). Surprisingly, however, studies of knockout (16, 17) and knock-in (15) mouse models of *HCN* genes have not demonstrated abnormal heart rates at rest or during β-adrenergic stimulation in adult animals.

Our study focused on the functional role of autonomic nervous system–mediated modulation of HCN channel activity via intracellular cAMP levels and its relevance to heart rate regulation. We generated transgenic mice with heart-specific and inducible expression of dominant-negative cAMP binding–deficient HCN4 subunits. In contrast to Harzheim et al. (15), who generated a similar cAMP-insensitive HCN4 subunit by mutating the cAMP-binding site of the CNBD (R669Q), we introduced a natural *HCN4* mutation (573X) that we had identified previously (12). Among the *HCN4* mutations identified to date, this mutation is unique, because the reported clinical symptoms include not only resting

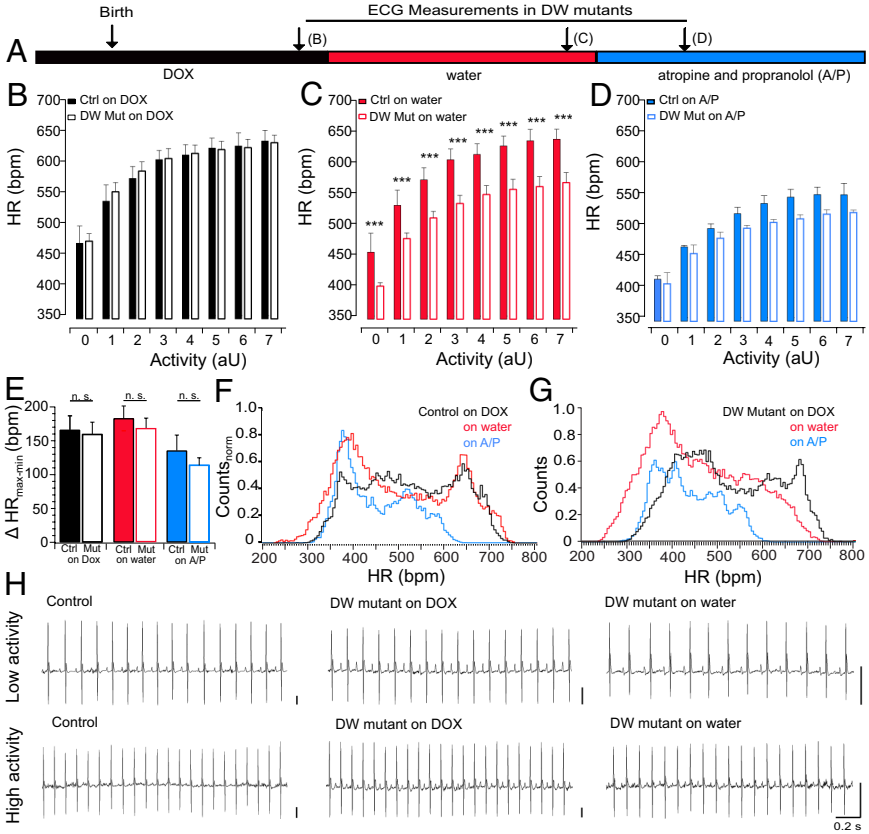

Fig. 5. Activity-dependent regulation of heart rate in control and mutant mice. (*A*) Experimental protocol. Mice were raised on DOX and implanted with telemetric devices. ECG recordings were obtained from the same animals raised on DOX (B), after withdrawal of DOX (water) (C), and during atropine and propranolol (A/P) administration (D). (*B*) Heart rate increased depending on the level of spontaneous home cage activity of control animals (filled bars; $n = 4$) and mutant animals on DOX (open bars; $n = 6$). (*C*) When hHCN4–573X expression was induced by DOX withdrawal (''on water''), the control mice exhibited the same activity-dependent heart rate as those raised on DOX. The mutant mice on water had a significantly lower heart rate at all activity levels. (*D*) Heart rates of controls and mutants during autonomic nervous system blockade with A/P. (*E*) Range of heart rate regulation calculated from the differences between maximum and minimum heart rates in (*B–D*). (*F* and *G*) Histogram of normalized average heart rates recorded during a 24-h period from control (*F*) and mutant (*G*; line A) mice on DOX (black), on water (red), and during autonomic nervous system blockade with A/P (blue). (*H*) Sample ECG raw traces (epochs of 2 s) from control and mutant animals on DOX or water at low and high physical activity levels showing reduced heart rate in mutants, but no signs of SAN dysfunction, conductance abnormalities, or ventricular arrhythmias. For quantification of PQ and QT_c interval durations, see Fig. S3. (Scale bars: 0.2 mV.) ***$P < .001$.

bradycardia (the key finding in most other patients with *HCN4* mutations), but also reduced maximum heart rate during exercise (12). hHCN4–573X confers cAMP insensitivity to coexpressed wild-type HCN subunits in a dominant-negative manner (12), comparable to the dominant effect of combined deletion of the C-linker (linking transmembrane domain S6 with the CNBD) and the CNBD in HCN2 channels (25). In contrast, the effect of R669Q in HCN4 (15) likely is comparable to the effect of the corresponding cAMP-binding site mutation R591E in HCN2, which does not completely eliminate the cAMP sensitivity of channels containing wild-type and R591E HCN2 subunits in a 1:1 stoichiometry (25).

Unlike Harzheim et al. (15), who generated $HCN4^{R669Q}$ knock-in mice constitutively expressing this cAMP binding–deficient HCN4 subunit throughout prenatal and postnatal life and in all HCN4-expressing tissues, we used the Tet-Off system to induce selective hHCN4–573X transgene expression in the hearts of adult animals. This was particularly important, because the embryonic lethality of homozygous $HCN4^{R669Q/R669Q}$ mice restricted the in vivo study by Harzheim et al. to heterozygous animals (15). One advantage of our approach is that transgene expression by DOX withdrawal is not induced before adulthood, preventing possible adaptive changes during development. Another advantage is that each animal may serve as its own control, because it can be recorded both without transgene expression while receiving DOX and with transgene expression after DOX withdrawal.

The presence of the hHCN4–573X transgene in isolated mutant SAN pacemaker cells rendered I_f completely insensitive to β-adrenergic stimulation, thereby causing a shift in both baseline and ISO-stimulated voltage dependencies by about −20 mV, resulting in a current activation threshold negative to the maximum diastolic potential. Interestingly, a previous study of cAMP-dependent regulation of native SAN f-channels predicted a −20-mV shift in the I_f activation curve from a switch from a saturating intracellular cAMP concentration to a cAMP-depleted intracellular environment (26). In line with this assumption, I_f in hHCN4–573X–expressing pacemaker cells activated in a negative voltage range, even at maximal ISO-mediated stimulation of the β-adrenergic receptor, as if no cAMP was present in the cell. Thus, in mutant cells, I_f was "frozen" in an activation range negative to that of the diastolic depolarization. Functionally, this negative shift corresponds to an almost complete loss of I_f activity at physiological SAN membrane voltages. The absence of a heart rate–lowering effect of IVA in the double-transgenic mutants is consistent with this conclusion. At the cellular level, spontaneous and regular firing of isolated SAN pacemaker cells was impaired. Some cells even failed to generate action potentials, instead exhibiting subthreshold membrane potential oscillations. Although I_f amplitudes were not increased by β-adrenergic stimulation, ISO application resulted in both a dose-dependent decrease in quiescent cells and a dose-dependent increase in spontaneous beating rates (although the

latter never reached control levels). The extent of the ISO-induced increase in firing rates observed in spontaneously active SAN cells was comparable in the mutants and controls, however. The marked reduction in spontaneous SAN cell firing rates associated with hHCN4–573X expression was mirrored in the telemetrically measured heart rates of intact conscious mutant mice. These animals had reduced basal heart rates at rest that increased with activity, but not to the levels seen in the same mice during DOX treatment or in control mice. Consistent with the cellular phenotype, the overall range of SAN frequency regulation (i.e., the difference between maximum and resting heart rates) was unchanged.

No SAN dysrhythmia [as present in *HCN2*$^{-/-}$ mice (17)] or SAN pauses [as present in adult *HCN4*$^{-/-}$ mice (16) or *HCN4*$^{+/R669Q}$ mice (15)] were observed in hHCN4–573X–expressing DW mutants. A likely explanation for this finding is that even in the absence of ISO, a few SAN cells beat regularly. This small pool of cells might be sufficient to maintain a regular sinus rhythm in the intact organism. Furthermore, in isolated mutant cells, ISO stimulation resulted in elevated spontaneous activity and a reduced number of silent cells. Because the adrenergic drive on SAN cells is significantly higher in an intact organism than in the culture dish, other cAMP-driven signaling pathways may compensate for the absence of I_f and thus contribute to the prevention of SAN failure. We found no evidence of any difference in ISO-induced diastolic currents in the presence of IVA between mutants and controls, so the exact mechanisms of this effect remain elusive.

Our data provide evidence that I_f plays a significant role in setting baseline and maximum SAN firing rates in adult mice by generating a voltage-dependent depolarizing "offset" current that is reflected in the slope of diastolic depolarization. These results explain the clinical phenotype of a patient with the same *HCN4* mutation that includes resting bradycardia and a reduced heart rate response to exercise (figure 1 in ref. 12). They also provide a biological rationale for the clinical efficacy of pharmacologic I_f blockade. The preserved relative extent of SAN frequency regulation against the background of "frozen" I_f activity also unambiguously demonstrates that I_f is not a prerequisite for heart rate regulation in adult mice. This finding may have therapeutic relevance, because the range of heart rate regulation in patients treated with IVA for heart rate reduction remains largely unchanged (27). In addition, our data demonstrate that pacemaker mechanisms other than I_f contribute significantly to the positive chronotropic effect of β-adrenergic stimulation by targeting effector molecules via protein kinase A or Ca^{2+} and calmodulin-dependent protein kinase II (CaMKII)-dependent pathways, such as $I_{Ca,L}$, I_{st}, I_{NCX}, and ryanodine receptor–mediated Ca^{2+} release (4, 5, 28).

In summary, our results demonstrate that cAMP-mediated modulation of I_f determines basal and maximal heart rates, but not the relative extent of SAN frequency regulation. Furthermore, our study reveals the pathophysiologic mechanism of hHCN4–573X–linked SAN dysfunction, paving the way for the generation of future mouse models for human diseases associated with impaired cardiac automaticity.

Materials and Methods

Generation of Transgenic Mice and Care and Use of Animals. See SI *Materials and Methods*.

Northern and Western Blot Analyses. RNA or proteins were isolated and analyzed using standard methods, as described in detail in SI *Materials and Methods*.

Electrophysiologic Recording of Pacemaker Activity and I_f in SAN Cells. The pacemaker activity of acutely isolated SAN cells was recorded at 35 °C under perforated-patch conditions; for details, see SI *Materials and Methods*.

ECG Telemetry and Analysis. For details, see SI *Materials and Methods*.

Statistics. Unless stated otherwise, data are expressed as mean ± SEM and were analyzed by ANOVA and Tukey's HSD posthoc test (Statistica; Statsoft).

ACKNOWLEDGMENTS. We thank I. Hermans-Borgmeyer for transgenic services, K. Sauter for technical assistance, H. Voss and the team of the ZMNH animal facility (Hamburg) and A. Cohen-Solal of the IFR3 animal facility (Montpellier) for animal care, B. Geertz for help with echocardiography, J. Faulhaber for help with ECG telemetry, O. Pongs and J. Nargeot for support, A. Marcantoni and E. Carbone for valuable discussions, T. Eschenhagen and A. Neu for critical comments on the manuscript, and all members of DFG-FOR604 for helpful discussions and criticism throughout the project. We also thank P. Seeburg and R. Sprengel for the Tet system indicator mice and the International Research Institute Servier (IRIS), France, for the generous supply of ivabradine. This project was supported by Deutsche Forschungsgemeinschaft Grant IS63/1–1/2 (to D.I. and H.E), Fondation de France (to M.M.), and Agence Nationale pour la Recherche Grant ANR-06-PHISIO-004–01 (to M.M.). P.M. is supported by CavNet, a Research Training Network funded through the European Union Research Program (6FP) (MRTN-CT-2006–035367).

1. Lamas GA, et al. (2000) The mode selection trial (MOST) in sinus node dysfunction: Design, rationale, and baseline characteristics of the first 1000 patients. *Am Heart J* 140:541–551.
2. Gillman MW, Kannel WB, Belanger A, D'Agostino RB (1993) Influence of heart rate on mortality among persons with hypertension: The Framingham Study. *Am Heart J* 125:1148–1154.
3. Fox K, et al. (2007) Resting heart rate in cardiovascular disease. *J Am Coll Cardiol* 50:823–830.
4. Maltsev VA, Lakatta EG (2008) Dynamic interactions of an intracellular Ca^{2+} clock and membrane ion channel clock underlie robust initiation and regulation of cardiac pacemaker function. *Cardiovasc Res* 77:274–284.
5. Mangoni M, Nargeot J (2008) Genesis and regulation of the heart automaticity. *Physiol Rev* 88:919–982.
6. Maltsev VA, Vinogradova TM, Lakatta EG (2006) The emergence of a general theory of the initiation and strength of the heartbeat. *J Pharmacol Sci* 100:338–369.
7. DiFrancesco D, Tortora P (1991) Direct activation of cardiac pacemaker channels by intracellular cyclic AMP. *Nature* 351:145–147.
8. Baruscotti M, Bucchi A, DiFrancesco D (2005) Physiology and pharmacology of the cardiac pacemaker (''funny'') current. *Pharmacol Ther* 107:59–79.
9. Nof E, et al. (2007) Point mutation in the HCN4 cardiac ion channel pore affecting synthesis, trafficking, and functional expression is associated with familial asymptomatic sinus bradycardia. *Circulation* 116:463–470.
10. Milanesi R, Baruscotti M, Gnecchi-Ruscone T, DiFrancesco D (2006) Familial sinus bradycardia associated with a mutation in the cardiac pacemaker channel. *N Engl J Med* 354:151–157.
11. Ueda K, et al. (2004) Functional characterization of a trafficking-defective HCN4 mutation, D553N, associated with cardiac arrhythmia. *J Biol Chem* 279:27194–27198.
12. Schulze-Bahr E, et al. (2003) Pacemaker channel dysfunction in a patient with sinus node disease. *J Clin Invest* 111:1537–1545.
13. Borer JS, Fox K, Jaillon P, Lerebours G (2003) Antianginal and anti-ischemic effects of ivabradine, an I_f inhibitor, in stable angina: A randomized, double-blind, multicentered, placebo-controlled trial. *Circulation* 107:817–823.
14. Leoni AL, et al. (2005) Chronic heart rate reduction remodels ion channel transcripts in the mouse sinoatrial node but not in the ventricle. *Physiol Genomics* 24:4–12.
15. Harzheim D, et al. (2008) Cardiac pacemaker function of HCN4 channels in mice is confined to embryonic development and requires cyclic AMP. *EMBO J* 27:692–703.
16. Herrmann S, Stieber J, Stockl G, Hofmann F, Ludwig A (2007) HCN4 provides a ''depolarization reserve'' and is not required for heart rate acceleration in mice. *EMBO J* 26:4423–4432.
17. Ludwig A, et al. (2003) Absence epilepsy and sinus dysrhythmia in mice lacking the pacemaker channel HCN2. *EMBO J* 22:216–224.
18. Yu Z, Redfern CS, Fishman GI (1996) Conditional transgene expression in the heart. *Circ Res* 79:691–697.
19. Gossen M, Bujard H (1992) Tight control of gene expression in mammalian cells by tetracycline-responsive promoters. *Proc Natl Acad Sci USA* 89:5547–5551.
20. Krestel HE, Mayford M, Seeburg PH, Sprengel R (2001) A GFP-equipped bidirectional expression module well suited for monitoring tetracycline-regulated gene expression in mouse. *Nucleic Acids Res* 29:E39.
21. DiFrancesco D, Camm JA (2004) Heart rate lowering by specific and selective I (f) current inhibition with ivabradine: A new therapeutic perspective in cardiovascular disease. *Drugs* 64:1757–1765.
22. DiFrancesco D (2006) Serious workings of the funny current. *Prog Biophys Mol Biol* 90:13–25.
23. Noma A, Morad M, Irisawa H (1983) Does the ''pacemaker current'' generate the diastolic depolarization in the rabbit SA node cells? *Pflügers Arch* 397:190–194.
24. Barbuti A, Baruscotti M, DiFrancesco D (2007) The pacemaker current: From basics to the clinics. *J Cardiovasc Electrophysiol* 18:342–347.
25. Ulens C, Siegelbaum SA (2003) Regulation of hyperpolarization-activated HCN channels by cAMP through a gating switch in binding domain symmetry. *Neuron* 40:959–970.
26. DiFrancesco D, Mangoni M (1994) Modulation of single hyperpolarization-activated channels I_f by cAMP in the rabbit sino-atrial node. *J Physiol* 474:473–482.
27. Joannides R, et al. (2006) Comparative effects of ivabradine, a selective heart rate–lowering agent, and propranolol on systemic and cardiac haemodynamics at rest and during exercise. *Br J Clin Pharmacol* 61:127–137.
28. Wu Y, et al. (2009) Calmodulin kinase II is required for fight-or-flight sinoatrial node physiology. *Proc Natl Acad Sci USA* 106:5972–5977.
29. Mangoni ME, et al. (2003) Functional role of L-type $Ca_v1.3$ Ca^{2+} channels in cardiac pacemaker activity. *Proc Natl Acad Sci USA* 100:5543–5548.
30. Mangoni ME, et al. (2000) Facilitation of the L-type calcium current in rabbit sinoatrial cells: Effect on cardiac automaticity. *Cardiovasc Res* 48:375–392.

Supporting Information

Alig et al. 10.1073/pnas.0810332106

SI Materials and Methods

Generation of Transgenic Mice. The Tet-responsive element (TRE-Tight) of pTRE-Tight (Clontech) was cloned into pWHERE2 v.01 (Invivogen). The complete ORF of hHCN4 (kindly provided by Benjamin Kaupp, Jülich, Germany; GenBank Accession NM_005477) was inserted downstream of Tre. A hemagglutinin epitope tag (YPYDVPDYA) was added to the N terminus of hHCN4 by PCR using pcDNA1-hHCN4, as described previously (1). The single-nucleotide deletion 1631delC was introduced in the HCN4 ORF by site-directed mutagenesis (1), yielding hHCN4–573X. All coding sequences were verified by direct sequencing. Transgenic mice carrying the pWHERE-Tre–hHCN4–573X construct were generated by pronuclear injection using standard techniques. Founder mice and the resulting offspring were genotyped by PCR using ear or tail biopsy specimens. Heart-specific promoter mice [FVB.Cg-Tg(Myh6-tTA)6Smbf/J] (2) were obtained from the Jackson Laboratories and backcrossed to the C57BL/6J strain for more than 4 generations. "Indicator" mice expressing GFP and β-galactosidase from a bidirectional DOX-sensitive module [Tg(GFPtetO7lacZ)] (3) were used to visualize αMHC-driven transgene expression.

Care and Use of Animals. Mixed genotype groups of each gender of no more than 5 animals were housed in standard mouse cages under specific pathogen-free conditions (12:12-h dark-light cycle, constant temperature, constant humidity, and food and water ad libitum). Double-transgenic mice and their tTA transgenic control littermates received either water alone or DOX-containing drinking water (200 μg/mL; Graymor Chemical) when breeding pairs were set up.

The care and use of animals and experimental procedures were in accordance with the German Law for the Protection of Animals and approved by the Ministry of Science and Public Health of the City State of Hamburg, Germany. The study design conforms to the U.S. National Institutes of Health's *Guide for the Care and Use of Laboratory Animals* (NIH Publication 85–23, revised 1996) and to European directives (86/609/CEE).

RNA Isolation and Northern Blot Analysis. Mice were deeply anesthetized and killed by cervical dislocation. Hearts were rapidly removed, washed with ice-cold PBS, flash-frozen in liquid nitrogen, and stored at -80 °C. Frozen heart tissue was pulverized in liquid nitrogen, homogenized in TRIzol reagent (Invitrogen), and processed according to the manufacturer's protocol. RNA samples (10 μg per lane) were separated by electrophoresis on a 1% agarose 0.35% formaldehyde gel and then transferred overnight by capillarity to a Hybond-N membrane (GE Healthcare). The RNAs were fixed on the membrane by baking at 80 °C for 1 h. The blot was prehybridized in 6× SSC, 2× Denhardt's solution, and 0.1% SDS for 2 h at 68 °C, after which an hHCN4-specific ^{32}P-labeled probe (25 ng) was added, and the blot was incubated overnight at 68 °C. The blot was washed for 20 min in 1× SSC, 0.1% SDS at room temperature and then twice in 0.2× SSC, 0.1% SDS at 68 °C. The membrane was exposed to a Kodak Biomax MR film (GE Healthcare) for 3 days at - 80 °C, then washed and rehybridized with 25 ng of a ^{32}P-labeled control GAPDH probe (4).

Protein Isolation and Western Blot Analysis. Frozen hearts were pulverized in liquid nitrogen and homogenized in 10% glycerol, 3% SDS, and 62.5 mM Tris (pH 6.8) containing a protease inhibitor mix (Sigma-Aldrich Chemie). Proteins were fractionated on NuPAGE 4%–12% Bis-Tris gels (Invitrogen) in NuPAGE Mops SDS running buffer (Invitrogen) and electrophoretically transferred to PROTRAN nitrocellulose membranes (Whatman). Western blot analysis was performed according to standard methods. Antibodies against HCN4 (Alomone Labs; 1:200 dilution) and calsequestrin (Affinity BioReagents; 1:2,500 dilution) were used as primary antibodies.

Isolation of SAN Cells. SAN pacemaker cells were isolated from control and mutant (founder line A) adult mice as described previously (5). Beating hearts were removed under general anesthesia consisting of 0.01 mg/g of xylazine (Rompun 2%; Bayer AG) and 0.1 mg/g of ketamine (Imalgène; Merial). The SAN region was excised in warmed (35 °C) Tyrode's solution containing 140.0 mM NaCl, 5.4 mM KCl, 1.8 mM $CaCl_2$, 1.0 mM $MgCl_2$, 5.0 mM Hepes-NaOH, and 5.5 mM D-glucose (adjusted to pH 7.4 with NaOH) and cut into tissue strips. These strips were transferred into a low-Ca^{2+}, low-Mg^{2+} solution containing 140 mM NaCl, 5.4 mM KCl, 0.5 nM $MgCl_2$, 0.2 mM $CaCl_2$, 1.2 mM KH_2PO_4, 50.0 mM taurine, 5.5 mM D-glucose, 1.0 mg/mL BSA, and 5.0 mM Hepes-NaOH (adjusted to pH 6.9 with NaOH). The tissue was enzymatically digested by adding 229 U/mL of collagenase type II (lot 49A26639; Worthington Biochemical), 1.9 U/mL of elastase (Roche Molecular Biochemicals), 0.9 U/mL of protease (Sigma), 1 mg/mL of BSA, and 200 μM $CaCl_2$. Tissue digestion was performed for 9–13 min at 35 °C with manual agitation using a flame-forged Pasteur pipette. Tissue strips were then washed and transferred into a medium containing 70.0 mM L-glutamic acid, 20.0 mM KCl, 80.0 mM KOH, 10.0 mM (±)D-β-OH-butyric acid, 10.0 mM KH_2PO_4, 10.0 mM taurine, 1 mg/mL BSA, and 10.0 mM Hepes-KOH 10.0 (adjusted to pH 7.4 with KOH). SAN myocytes were manually dissociated in KB solution at 35 °C for about 10 min. Cellular automaticity was recovered by readapting the cells to physiological extracellular Na^+ and Ca^{2+} concentrations by adding aliquots of solutions containing 10.0 mM NaCl and 1.8 mM $CaCl_2$, and then normal Tyrode's solution containing 1 mg/mL BSA. The final storage solution contained 100.0 mM NaCl, 35.0 mM KCl, 1.3 mM $CaCl_2$, 0.7 mM $MgCl_2$, 14.0 mM L-glutamic acid, 2.0 mM (±)D-β-OH-butyric acid, 2.0 mM KH_2PO_4, 2.0 mM taurine, and 1.0 mg/mL BSA (pH 7.4). Cells were then stored at room temperature until use. All chemicals were obtained from Sigma except for the (±)D-β-OH-butyric acid, which was obtained from Fluka Chemika.

Electrophysiological Recording of Pacemaker Activity and I_f in SAN Cells. The pacemaker activity of SAN cells was recorded at 35 °C under perforated-patch conditions by adding 30 μM β-escin (6) to the pipette solution. The extracellular Tyrode's solution contained 140.0 mM NaCl, 5.4 mM KCl, 1.8 mM $CaCl_2$, 1.0 mM $MgCl_2$, 5.0 mM Hepes-NaOH, and 5.5 mM D-glucose (adjusted to pH 7.4 with NaOH). The cell action potential was recorded using an intracellular solution containing 130.0 mM K^+-aspartate, 10.0 mM NaCl, 2.0 mM ATP-Na^+ salt, 6.6 mM creatine phosphate, 0.1 mM GTP-Mg^{2+}, 0.04 mM $CaCl_2$ (pCa 7.0), and 10.0 mM Hepes-KOH (adjusted to pH 7.2 with KOH). The rate of SAN cell pacemaker activity was calculated by counting the number of action potentials in segments of 1-min duration under basal conditions and after application of ISO. The total basal and ISO-induced membrane current was measured by applying a train of digitized action potentials starting

from a holding membrane potential of -80 mV (Fig. S2*A*). The train of action potentials was generated by digitizing a representative current clamp recording of a control SAN cell. Membrane series resistance was routinely compensated for electronically up to 90%. The cell membrane capacitance was monitored by applying brief (10 ms) voltage steps of ± 10-mV amplitude from a holding potential of -35 mV. Membrane capacitance was calculated according to

$$C_m = \tau/Rs, \quad [1]$$

where C_m is the membrane capacitance, τ is the decay time constant of the membrane capacitance transient, and $R_s = \Delta V/I$, where ΔV is the step amplitude and I is the maximum current level. The value of C_m was used to estimate I_f current density in each cell.

Analysis of I_f was performed as described previously (5). Changes in current were thus described according to

$$I_f(V, t) = I_f P(V, t), \quad [2]$$

where V is the voltage, t is the time, and P is the activation variable. In eq. (2), the activation variable P satisfies the Boltzmann relation

$$P(V) = 1/1 + \exp((V - V_{1/2})/s), \quad [3]$$

where $V_{1/2}$ is the voltage for current half-activation and s is the slope factor.

Activation time constants were calculated by fitting single-exponential equations to experimental traces,

$$I_f A \exp(-(t - t_0)/\tau_{act}), \quad [4]$$

where A is a fixed factor, t is time, and t_0 represents the onset of current activation.

All fits were performed by numerical iteration using a Levenberg-Marquardt–based numerical algorithm (Origin 7.5 built-in). All results are presented as mean ± SEM.

ECG Analysis. For ECG telemetry, male mice ranging in age from 3 to 4 months were anesthetized with isoflurane and implanted with PhysioTel EA-F20 mouse transmitters (Data Sciences International). Atropine (15 mg/kg body weight/day) and propranolol (5 mg/kg body weight/day) were administered using an osmotic minipump (Alzet; Charles Rivers Laboratories), to avoid handling-induced changes in heart rates. Before undergoing ECG, the mice were allowed to recover for at least 1 week after implantation of the telemetry device and for 2 days after minipump implantation. ECG data were continuously acquired for each animal for at least 72 h using a sampling rate of 1 kHz. Heart rate and cage activity were calculated using 1-minute moving averages from continuous ECG recordings analyzed with Dataquest ART 2.3 (Data Sciences International). Arbitrary activity counts (usually 0–30 aU) were calculated by the recording system (Data Sciences International) as a function of alterations in transmitter signal strength, which changes with locomotor activity, and binned for analysis, with a bin width of 5 counts. The mean heart rate was determined separately for each animal and activity bin, to ensure that each animal had the same weight in the statistical analyses (Fig. 5*B–D*).

For the analysis of ECG parameters, 6 ECG epochs of 1 min each per animal and treatment (i.e., DOX, water, and autonomic nervous system blockade) were selected at low activity level (0 aU) and high activity level (>25 aU). PQ and QT_c (7) interval durations were determined using Chart 5 (ADInstruments). Two-way ANOVA and Tukey's honest significant differences (HSD) posthoc test (Statistica; Statsoft) were used for statistical comparison of repetitive measurements in individual mice and subsequent group analysis.

Echocardiography. Two-dimensional echocardiography images were obtained in a modified parasternal long-axis view and a short-axis view at the midpapillary muscle level at a frame rate of 60 Hz (VisualSonics Vevo 660). Mice were kept under light anesthesia (isoflurane 1.8–2.0 vol %) with continuous temperature and ECG monitoring. Echocardiographic studies were performed before and after i.p. injection of the β-agonist dobutamine (10 μg/g; Carinopharm). Epicardial and endocardial areas of the left ventricular cavity were obtained in a short-axis view during diastole and systole. Area shortening (AS) was calculated by

$$\%AS = (\text{LV end-diastolic area} - \text{LV end-systolic area})/\text{LV end-diastolic area}. \quad [5]$$

Left ventricular end-diastolic diameter (LVEDD) was obtained in the long-axis view. Left ventricular end-diastolic volume (LVEDV) was calculated as

$$\text{LVEDV } (\mu L) = 5/6\ (\text{LVEDD})(\text{LV end-diastolic area}). \quad [6]$$

Left ventricular mass (LVM) was calculated as

$$\text{LVM} = [1{,}05\ (5/6\ A1*(L + t) - 5/6\ A2*L)], \quad [7]$$

where A1 and A2 are the epicardial and endocardial areas, respectively, acquired in a short-axis view, L is the LV diameter (long axis), and t is wall thickness (8).

1. Schulze-Bahr E, et al. (2003) Pacemaker channel dysfunction in a patient with sinus node disease. *J Clin Invest* 111:1537–1545.
2. Yu Z, Redfern CS, Fishman GI (1996) Conditional transgene expression in the heart. *Circ Res* 79:691–697.
3. Krestel HE, Mayford M, Seeburg PH, Sprengel R (2001) A GFP-equipped bidirectional expression module well suited for monitoring tetracycline-regulated gene expression in mouse. *Nucleic Acids Res* 29:E39.
4. Matsui Y, Zsebo KM, Hogan BL (1990) Embryonic expression of a haematopoietic growth factor encoded by the Sl locus and the ligand for c-kit. *Nature* 347:667–669.
5. Mangoni ME, Nargeot J (2001) Properties of the hyperpolarization-activated current I_f in isolated mouse sino-atrial cells. *Cardiovasc Res* 52:51–64.
6. Fan JS, Palade P (1998) Perforated patch recording with beta-escin. *Pflügers Arch* 436:1021–1023.
7. Mitchell GF, Jeron A, Koren G (1998) Measurement of heart rate and Q-T interval in the conscious mouse. *Am J Physiol* 274(3 Pt 2):H747–H751.
8. Collins KA, Korcarz CE, Lang RM (2003) Use of echocardiography for the phenotypic assessment of genetically altered mice. *Physiol Genomics* 13:227–239.

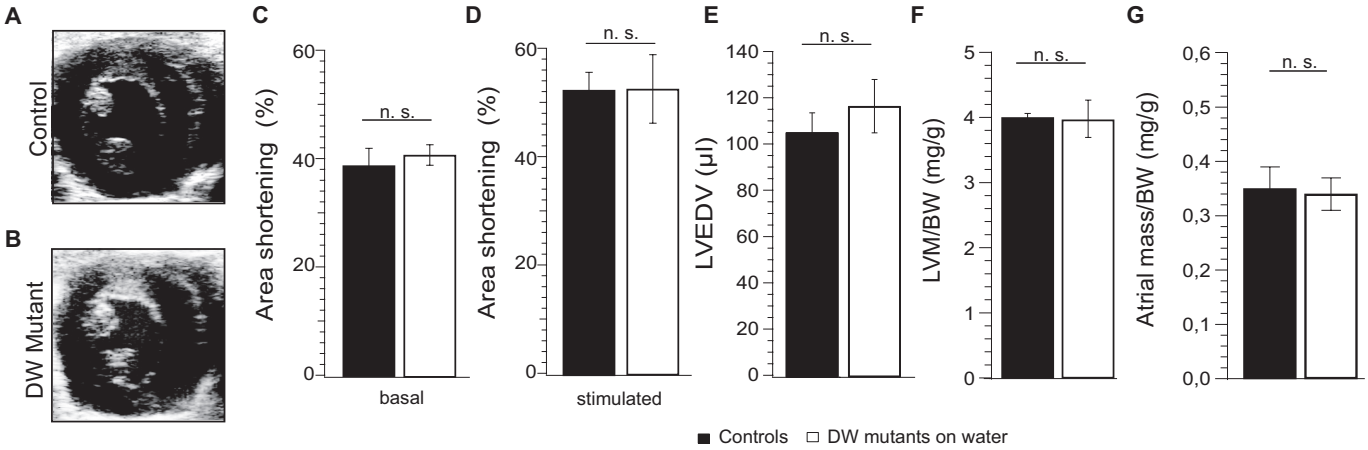

Fig. S1. Ventricular size and function were normal in control and mutant mice independent of expression state or level. (*A* and *B*) Representative example images acquired by in vivo echocardiography along the short cardiac axis of a control mouse (*A*) and a mutant mouse (*B*; line A). (*C*–*G*) No differences in area shortening at baseline (*C*) or after stimulation with dobutamine (*D*), LVEDV (*E*), LVM-to-body weight ratio (*F*), or atrial mass-to-body weight ratio (*G*) were seen between the control ($n = 6$) and mutant animals ($n = 6$). Data are given as mean ± SEM and were compared using the Student *t* test (n.s., not significant).

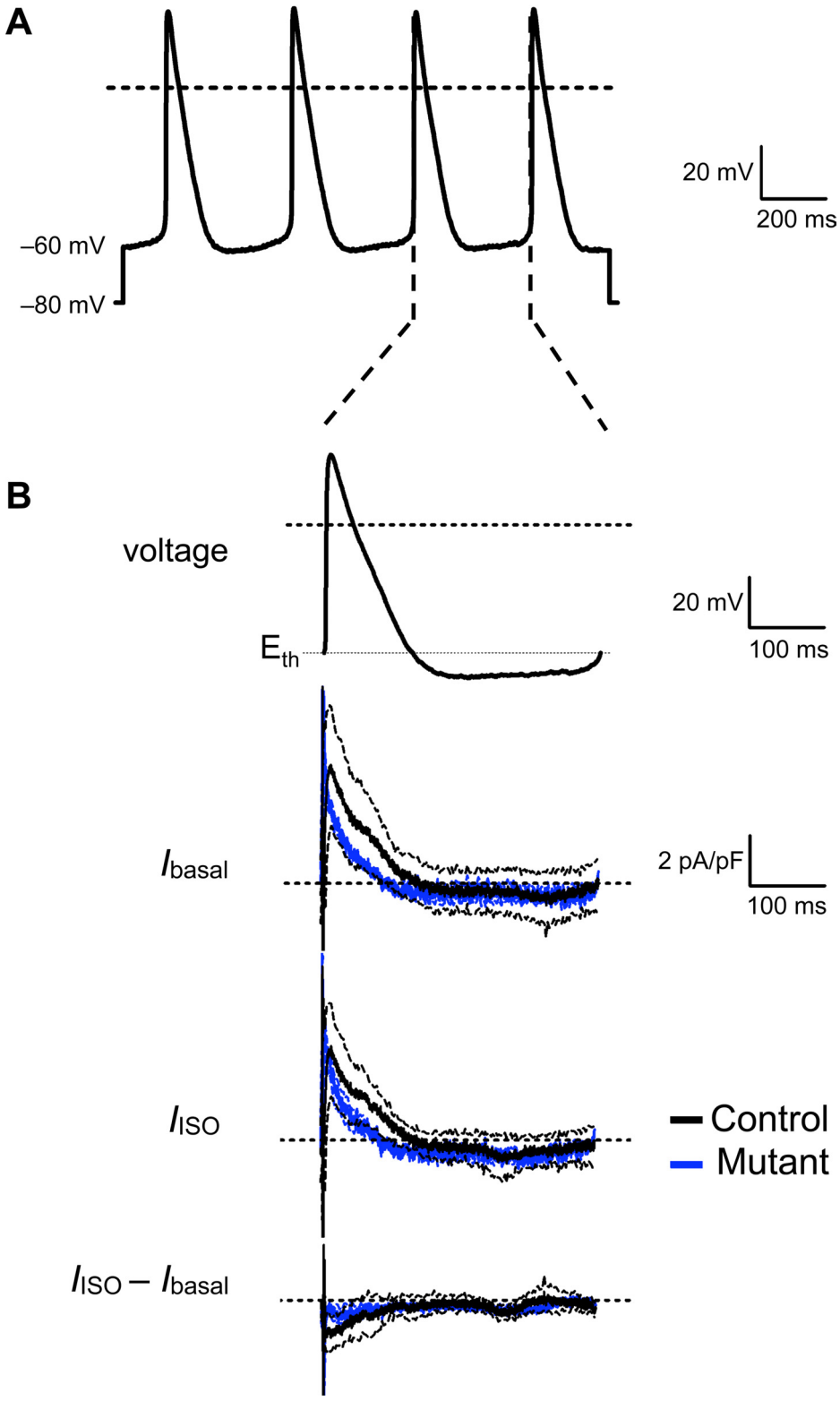

Fig. S2. ISO-induced total membrane currents of control and mutant SAN cells. (*A*) A short train of digitized control SAN cell action potentials was used as a voltage-clamp protocol to analyze the resulting membrane currents in control (black line; $n = 5$) and mutant (blue line; $n = 4$) SAN cells. The membrane current was analyzed after steady state was achieved (i.e., from the threshold of the third action potential to that of the following action potential); see the dashed line enlargement. (*B*) The top panel shows the membrane voltage range used for analysis. The other panels show mean net membrane currents under control conditions (I_{basal}) and after perfusion of 100 nM ISO (I_{ISO}), and the mean difference currents (I_{ISO} - I_{basal}), which represent a quantitative measure for ISO-induced currents. Dashed lines represent the respective SEM. No significant differences are seen at reference points 0 and -20 mV (*t* test; $P > .05$).

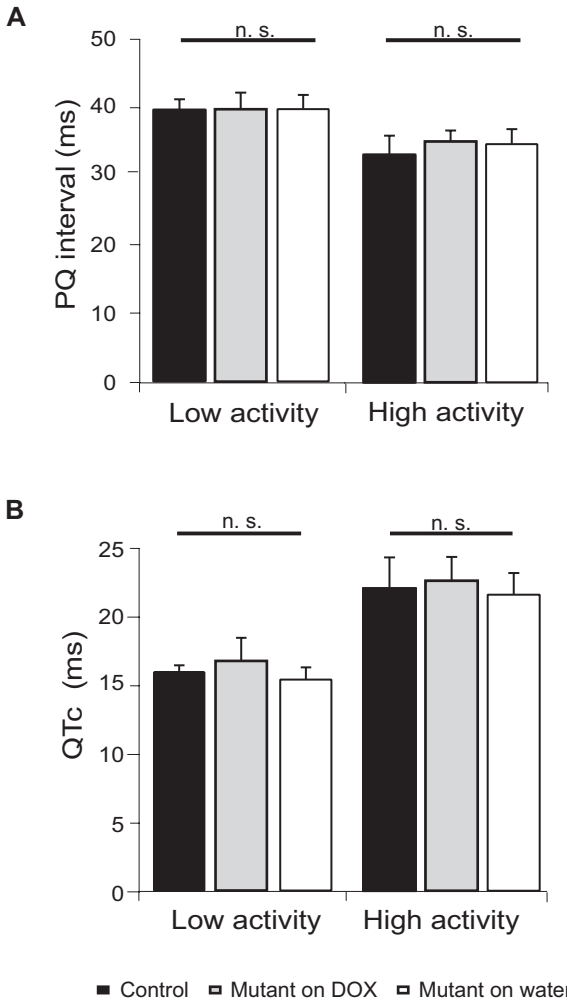

Fig. S3. ECG parameters of DW mutants remained unchanged. Transgene expression in adult DW mutants was induced by DOX withdrawal. Analysis of ECG parameters of the same animals shown in Fig. 5 revealed no changes in either PQ (*A*) or QT_c (*B*) interval durations. Data are given as mean ± SEM and were compared using 2-way ANOVA and Tukey's HSD posthoc test (n.s., $P > .05$).

Table S1. β-adrenergic regulation of pacemaker activity in SAN cells

		Controls			Mutants		
		Baseline	2 nM ISO	100 nM ISO	Baseline	2 nM ISO	100 nM ISO
Rate, bpm		231 ± 21	275 ± 20	325 ± 20	117 ± 35	188 ± 35	232 ± 43
P	Control (baseline)		.146	.0002	.0001	.117	.997
	Control (2 nM ISO)			.080	.0001	.0003	.067
	Control (100 nM ISO)				.0001	.0001	.0002
	Mutant (baseline)					.011	.0002
	Mutant (2 nM ISO)						.334

Application of ISO at concentrations of 2 and 100 nM led to a dose-dependent increase in the spontaneous firing rates of control ($n = 12$) and mutant ($n = 10$) SAN cells; however, in SAN cells, a saturating dose of ISO (100 nM) had to be added to achieve a pacing rate similar to the basal (unstimulated) rate of control cells. Data are expressed as mean ± SEM and were analyzed by ANOVA and Tukey's HSD post hoc test.